Visible Light Curing of Epon SU-8 Based Superparamagnetic Polymer Composites with Random and Ordered Particle Configurations

Christian Peters,[*][†] Olgaç Ergeneman,[‡][#] Georgios A. Sotiriou,[§][⊥] Hongsoo Choi,[∥][∞] Bradley J. Nelson,[‡][×] and Christofer Hierold[†][○]

[†]Micro and Nanosystems, Department of Mechanical and Process Engineering, ETH Zurich, Tannenstrasse 3, 8092 Zurich, Switzerland

[‡]Institute of Robotics and Intelligent Systems, Department of Mechanical and Process Engineering, ETH Zurich, 8092 Zurich, Switzerland

[§]Particle Technology Laboratory, Department of Mechanical and Process Engineering, ETH Zurich, 8092 Zurich, Switzerland

[∥]Robotics Engineering Department, DGIST-ETH Microrobot Center, Daegu Gyeongbuk Institute of Science and Technology (DGIST), Daegu, Korea

ABSTRACT: The performance of superparamagnetic polymer composite microdevices is highly dependent on the magnetic particle content. While high loading levels are desired for many applications, the UV absorption of these nanoparticles limits the overall thickness of the fabricated microstructures and subsequently their capability of magnetic interaction. The combination of a visible-light-sensitive photoinitiator and particle self-organization is proposed to extend the exposure depth limitation in Epon SU-8 based superparamagnetic polymer composites. While superparamagnetic iron oxide particles strongly absorb i-line radiation

required to cross-link the Epon SU-8 polymer matrix, we propose the utilization of H-Nu 470 photoinitiator to expand the photosensitivity of the composite toward the visible spectrum, where the dispersed nanoparticles are more transparent. The novel photoinitiator preserves the composite's superparamagnetic properties as well as a homogeneous particle distribution. As a result, particle load or resist thickness can be more than doubled while maintaining exposure time. The self-organization of ordered magnetic structures allows for an additional increase in exposure depth of up to 40%, resulting in a 2.5-fold saturation magnetization.

KEYWORDS: superparamagnetic polymer composite, lithography, visible light curing, H-Nu 470, magnetite
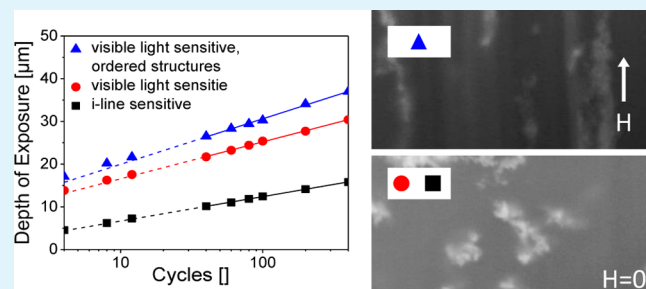
INTRODUCTION

The diversity of material properties of polymers has attracted great attention in the micro- and nanofabrication community and led to the development of various polymer-based sensors and actuators.[1,2] The combination of different polymer materials into copolymers and polymer blends can be applied to alter mechanical properties of these devices.[3] Inherently different material properties can be obtained by the incorporation of organic and inorganic filler materials into the polymer network. On the basis of this approach, Jiguet et al. demonstrated conductive polymer composites by dispersing silver nanoparticles into an Epon polymer matrix.[4] Vescovo et al. reported silver/epoxide composites fabricated by the in situ synthesis.[5] Jiguet et al. also demonstrated the dispersion of silica nanoparticles in order to reduce residual stress in cross-linked Epon polymer films.[6] Garcia et al. demonstrated anisotropic reinforcement of a cured polymer matrix by dispersing and aligning carbon nanotubes.[7] Lo et al. demonstrated ordered arrangements of magnetic nanorods dispersed in microphase-separated diblock copolymers.[8]

Metwalli et al. as well as Yao et al. demonstrated hybrid nanoparticle polymer films with ordered particle configurations.[9−11]

Suter et al. and Peters et al. demonstrated the incorporation of superparamagnetic iron oxide nanoparticles into an Epon SU-8 polymer matrix, enabling remote actuation of cantilevers and untethered swimming microrobots by applying magnetic force and torque, respectively.[12−15] The magnetic force/torque that can be exerted on these actuators depends on the strength of the external magnetic field, the actuator volume, and the actuator magnetization.[16] The strength of the external magnetic field is generally limited by the magnetic setups. Subsequently, magnetic force and torque may only be increased by increasing the overall device volume, i.e., thickness, or device magnetization, which is related to the particle load.[12]

A general problem during lithographic processing of Epon-based superparamagnetic composites is that the dispersed particles absorb i-line radiation required to initiate the cross-linking process and, thus, limit exposure depth and particle load. For instance, Suter et al.[17] and Gach et al.[18] demonstrated Epon composite thicknesses and maximum particle loads of 2.9 μm/5% vol and 12 μm/1% vol, respectively. As a consequence, the performance of superparamagnetic composite actuators is greatly reduced in comparison to those fabricated from bulk magnetic material.[12,19]

To fabricate more competitive superparamagnetic composite sensors and actuators, the nanoparticle-induced UV absorption must be overcome or avoided. As the particle-induced absorption of the filler materials decreases with increasing wavelength,[12] expanding the composite's photosensitive region toward the visible spectrum is expected to increase the penetration depth of the photoactive radiation, enabling an increased film thickness and particle load. While visible light curing of pristine Epon has been established over a decade ago,[20,21] visible light curing of Epon nanocomposites has been neglected, to date.

Lv et al. as well as Xuan et al. investigated the optical transmission of superparamagnetic ferrofluids (non-cross-linked) subjected to homogeneous magnetic fields.[22,23] They identified particle absorption as the main attenuation mechanism and argued that the overall film absorption is dependent on the spatial distribution of the particles. In the presence of external magnetic fields, the dispersed nanoparticles are magnetized and form chains along the direction of the external magnetic field. If the direction of the incident light coincides with the orientation of the particle chains, the cross-sectional area which is occupied by the particles is reduced and absorption incidents are less likely to occur. Increased transmission in the direction of the aligned particles was observed experimentally for micrometer wavelengths. Similar behavior is expected for shorter wavelengths and must result in an additional increase in curing depth.

In this work, we investigate the potential of the visible light sensitive photoinitiator H-Nu 470 as well as directed particle self-organization in order to increase the photopatternable resist thickness of a previously developed Epon based superparamagnetic polymer composite. Optical properties of the proposed photoinitiator H-Nu 470, Epon SU-8, as well as the ferrofluid are investigated by UV–vis spectroscopy and related to a first-order cationic photocuring model. Photosensitive polymer composites with different particle loading levels and different photoinitiators are prepared and cross-linked in the absence and presence of external magnetic fields. The related composite curing rates are evaluated and the magnetic properties of cross-linked films are characterized by a vibrating sample magnetometer (VSM). The particle distribution is investigated by preparing focused ion beam (FIB) cuts.

Photoresist Cross-Linking. Cationic cross-linking of a chemically amplified photoresist consists of four steps: exposure of the photosensitive component, photoacid generation, photoacid diffusion, and chemical amplification as well as network formation during postexposure bake.[24] The irradiation intensity distribution $I(z)$ within the exposed composite film is given by:

$$I(z) = I_0 \exp(-\alpha z) \tag{1}$$

where I_0 is the irradiation intensity at the composite surface, α is the overall composite absorption coefficient, and z is the depth from the composite surface. Provided that the absorptions of the composite's components do not influence each other, the overall composite absorption α is defined as the sum of its component's absorption coefficients:[25]

$$\alpha = \alpha_{\text{SU-8}} + \alpha_{\text{Particles}} + \alpha_{\text{H-Nu}} \tag{2}$$

where $\alpha_{\text{SU-8}}$ is the absorption coefficient of the Epon SU-8 photoresist that includes its standard photoinitiator components, $\alpha_{\text{Particles}}$ is the absorption coefficient of the dispersed nanoparticles, and $\alpha_{\text{H-Nu}}$ is the absorption coefficient of the proposed photoinitiator H-Nu 470. The concentration of the generated photoacid $H(z)$ is related to the intensity distribution $I(z)$:

$$H(z) = G_0[1 - \exp(-CI(z)t)] \tag{3}$$

where G_0 is the initial photoacid generator concentration, C is the exposure rate constant, and t is the exposure time. The characteristic of the chemical amplification is that the photoacid acts as a catalyst during cross-lining and is therefore not consumed, i.e., one photoacid molecule can lead to several cross-linking events with typical numbers between 10 and 100.[24] Neglecting photoacid diffusion, a minimum photoacid concentration $C_{\text{threshold}}$ is required to allow for sufficient cross-linking:

$$\frac{H(z)}{G_0} \geq C_{\text{threshold}} \tag{4}$$

The absorption coefficients in eq 2 are wavelength dependent and have to be regarded at the relevant wavelengths. A wavelength is referred to as relevant if it is emitted by mask aligner's light source and can generate a photoacid within the composite at the same time. There are three characteristic wavelengths emitted by the utilized mask aligner (Karl Suss MA-6 with UV 400 optics, Munich/Germany): g-line (436 nm), h-line (405 nm), and i-line (365 nm). The Epon SU-8 photoacid generator triarylsulfonium (SbF_6) is only i-line sensitive, and composites containing this initiator possess only one relevant wavelength. H-Nu 470 photoinitiator is photosensitive beyond 500 nm wavelength. g-, h-, and i-line wavelengths are considered relevant wavelengths for composites containing H-Nu 470 photoinitiator.

Absorption coefficients and intensity distributions are combined to analytically describe the overall photoresist conversion utilizing eqs 1–4. Mathematical treatment can be simplified if dominant effects are identified. Dominant effects result from a small absorption coefficient in combination with a high radiation intensity. Both effects are linked, and only one of the two effects needs to be significant; i.e., if two wavelengths possess similar irradiation intensities, the wavelength at which the composite possesses the smaller absorption coefficient is considered dominant.

Deriving eqs 1–4 for two composites (denoted 1 and 2) equipped with the same photoinitiator but different particle loads yields:

$$\alpha_1 \, \text{DOE}_1 = \alpha_2 \, \text{DOE}_2 \tag{5}$$

where DOE is the depth of exposure, equivalent to the thickness of the fully cross-linked composite film. Assuming that α is directly proportional to the volume load of the particles, Load_V, eq 5 can be rewritten as:

$$\text{Load}_{V,1} \, \text{DOE}_1 = \text{Load}_{V,2} \, \text{DOE}_2 \tag{6}$$

Table 1. Formulation of Epon Su-8 5 Reference Photoresist and Superparamagnetic Poylmer Composites Investigated in This Work[a]

composite	Epon [% wt]	GBL [% wt]	SBF$_6$ [% wt]	H-Nu 470 [% wt]	OPPI [% wt]	AN-910-E [% wt]	magnetite [% wt]	Load$_{V,i}$ [% vol][b]
SU-8 5	50.00	47.50	2.50					0
1	46.76	46.76	2.35				4.13	2
2	43.90	43.90	2.21				9.99	5
3	39.52	39.52	1.98				18.98	10
4	45.99	45.99	2.31	0.04	1.15	0.46	4.06	2
5	43.22	43.22	2.17	0.04	1.08	0.43	9.39	5
6	38.96	38.96	1.96	0.04	0.97	0.39	18.72	10

[a]Composites 1, 2, and 3 are senstive to i-line irradioation because of the presence of triarylsulfonium salt (SbF$_6$). Composites 4, 5, and 6 are senstive to broadband irradiation from g-, h-, and i-line because of the presence of the H-Nu 470 PI system (H-Nu 470 + OPPI + AN-910-E). [b]See eq 9.

The volume of a cross-linked Epon network is known to undergo changes based on the processing conditions.[26] Subsequently, it is imperative to determine the apparent particle volume load based on the cross-linked network using:

$$\text{Load}_V = \frac{M_r}{M_R A \text{ DOE}} = \frac{M_V}{M_R} \tag{7}$$

where M_r is the relative saturation magnetization of the composite film [emu], M_R is the reference saturation magnetization of the iron oxide nanoparticles [emu/cm^3], A is the sample surface area, and M_V is the volume saturation magnetization of the composite film. Applying eq 7 to both sides of eq 6 yields:

$$M_{r,1} = M_{r,2} \tag{8}$$

If α is directly proportional to the volume load of the particles Load$_V$, the relative sample saturation magnetization of two composite samples containing different particle loads but the same photoinitiator must be equal.

Particle Distribution and Self-Organization. Surfactant-coated superparamagnetic nanoparticles possess a homogeneous particle distribution throughout the ferrofluid as well as the cross-linked composite.[12] When a magnetic field is applied during composite processing, the dispersed particles are magnetized, leading to attractive forces between these particles, initiating the formation of particle chains along the direction of the external field.[13] Lv et al. simulated the dynamics of particle chain formation in non-cross-linked ferrofluids and suggested that the particle chains become more pronounced with time until they reach an equilibrium. As the composite's solvent evaporates during processing, the particle mobility decreased to zero and an equilibrium state may not be reached. As the evaporation time depends on the diffusion length, i.e., the thickness of the spin-coated composite film, particle mobility is expected to be maintained in thicker composite films, leading to a more pronounced formation of particle chains.

■ EXPERIMENTAL SECTION

Superparamagnetic Ferrofluid. The superparamagnetic Epon composite discussed in this work is derived from a superparamagnetic FerroFluid (FF) developed in collaboration with ChemiCell GmbH (Berlin, Germany).[12] The FF consists of superparamagnetic magnetite nanoparticles (Fe$_3$O$_4$, 11 nm average particle diameter, measured by TEM[12]) dispersed in γ-butyrolactone (GBL) with a particle concentration of 260 mg/mL.

UV–Visible Spectroscopy. In order to assess the optical properties of utilized nanoparticles, the UV–vis spectrum of the magnetite FF was recorded using a Varian Cary 500 spectrometer. A 1% vol FF was prepared and further diluted with GBL (puriss., ≥99.0% (GC) (Fluka), Sigma-Aldrich, Switzerland) in ratios of 1/

1000, 1/2000, and 1/4000 in order to allow for a detectable UV–vis signal. All UV–vis measurements were performed against a GBL background signal.

Superparamagnetic Polymer Composite. *Depth Cure.* The i-line sensitive polymer composites were obtained by dispersing the FF in commercial Epon-based photoresist (commercial name: "SU-8", purchased from Micro Resist Technology GmbH, Berlin, Germany). The composition of the pristine photoresist is depticted in Table 1. Particle dispersion is carried out using a Hauschild DAC 150 planetary mixer for 10 min and sonicated in a Sonics & Materials Inc. Vibracell VCX 600 ultrasound system for 20 min. The particle content was adjusted to achieve initial volume loads Load$_{V,i}$ of 2% vol, 5% vol, and 10% vol with respect to the solid Epon resin volume:

$$\text{Load}_{V,i} = \frac{V_{\text{Particles}}}{V_{\text{Particles}} + V_{\text{Epon}}} \tag{9}$$

where $V_{\text{Particles}}$ is defined as the particle volume and V_{Epon} represents the volume of the Epon resin. Please note that the initial volume load (eq 9) differs from the particle load of the cross-linked composite (eq 7). This discrepancy is attributed to the fact that the Epon volume changes during device fabrication. The composites contain triarylsulfonium salt (SbF$_6$, standard Epon SU-8 photoacid generator; see Table 1) and are only sensitive to i-line irradiation.[27]

Depth Cure. Visible light sensitive polymer composites are obtained by dispersing the FF in commercial Epon SU-8 photoresist as denoted above. Additionally, a visible light sensitive curing system consisting of H-Nu 470 PI (5,7-diiodo-3-butoxy-6-fluorone), OPPI photoacid generator (4-(octyloxy)phenylphenyliodium hexafluoroantimonate), and AN-910-E cationic cure accelerator was added. All PI components were purchased from Spectra Group Limited (Millbury, OH, U.S.). The component's weights were adjusted to achieve concentrations of 0.1% wt, 2.5% wt, and 1.0% wt with respect to Epon mass, respectively. Three visible light sensitive polymer composites with initial volume load of 2% vol, 5% vol, and 10% vol were prepared. The exact formulation of all six composites investigated in this work is depicted in Table 1.

Radiation Intensity Measurements. All composites discussed in this work were exposed using a Karl Suss MA-6 mask aligner equipped with a mercury short-arc lamp and UV-400 optics, emitting g-, h-, and i-line radiation. The mask aligner was operated in constant power mode. Radiation intensities were measured using a transimpedance photoamplifier equipped with hard-coated, narrow-band UV filters and an optical attenuator. The transmission properties of the filters as well as transmission properties of the attenuator have been obtained using a Varian Cary 500 spectrometer.

Evaluation of Exposure Kinetics. All composites were spin-coated on chrome-patterned, rectangular 38 mm glass wafers at 1000 rpm for 30 s. The low spin-coating speed was selected to produce composite films that are thicker than the maximum DOE after 400 exposure cycles. The samples were then soft-baked for 1 h at 95 °C, placed upside down on a silicon carrier wafer, and exposed from the back side. The silicon wafer caps the composite surface and inhibits oxygen diffusion into the composite film during exposure. After defined numbers of exposure cycles, i.e., 4, 8, 12, 40, 60, 80, 100, 200,

and 400, selected parts of the wafer were covered by silicon die in order to monitor the DOE progress on a single wafer. A schematic illustration of the sample preparation is depicted in Figure 1.
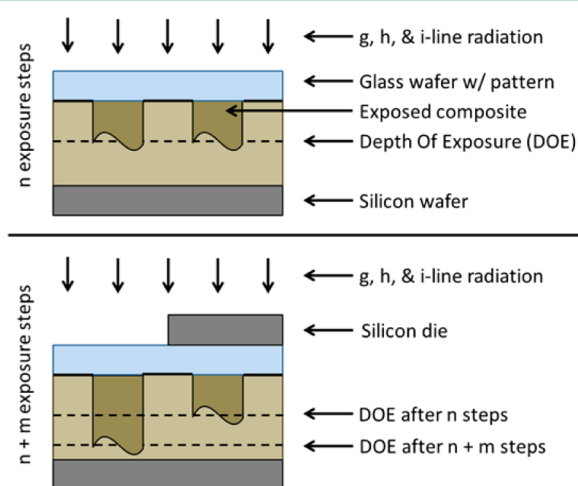
Figure 1. Back-side exposure of Epon nanoparticle composite spin-coated on a chrome-patterned glass wafer. Depth of exposure (DOE) increases with increasing number of exposure cycles. Reprinted with permission by © IEEE 2013 (modified version).

Postexposure bake was carried out for 15 min at 95 °C. Non-cross-linked composite was removed using mr-Dev 600 developer (Micro Resist Technology GmbH, Berlin, Germany). Developed samples were rinsed with isopropanol as well as DI water and dried with nitrogen. The particle distribution in all these films is random. The related DOE profiles were recorded using a Tencor P10 surface profiler.

Evaluation of Magnetic Properties. For the evaluation of magnetic properties, all composites were spin-coated on circular, transparent 9 mm glass wafers. All process steps were carried out as denoted above except that no parts of the wafer were covered and that the soft bake was carried out for 4 h. The exposure dose matched the maximum exposure dose of the previous experiments. Samples for reference magnetization measurements were prepared by drop casting the ferrofluid on a circular glass wafer and subsequent evaporation of the composite solvent. Sample magnetization has been recorded using a Princeton Measurements Corp. MicroMag 3900 VSM. After characterization of the magnetic properties, the composite films were partially scratched to obtain a step profile. Film thickness was measured using white light interferometry and profilometry on these steps.

Particle Manipulation. Particle manipulation was carried out using composites equipped with the visible light sensitive photo-initiator system H-Nu 470 only. After composite spin-coating, the wafers were transferred to a custom Helmholtz setup, generating a homogeneous magnetic field of 30 mT perpendicular to the wafer surface. The Helmholtz coil setup is equipped with a hot plate in order to combine particle alignment and thermal cycling. The soft-baked samples were exposed and transferred back to Helmholtz setup for postexposure bake. Non-cross-linked composite was removed using mr-Dev 600 developer. All process parameters were used as denoted above.

Particle Distribution Characterization. The particle distribution has been characterized by preparing FIB cuts of all composite films. The cross sections of these samples were assessed using a Hitachi NB5000 FIB SEM. For all experiments, composite films fabricated on circular wafers were used.

■ RESULTS

Radiation Intensity Distribution, Absorption Characteristics, and Its Implications. The absorption characteristics of the utilized FF (magnetite nanoparticles dissolved in GBL)

are illustrated in Figure 2 for three different dilution ratios. A Beer–Lambert relation is observed for these low concen-
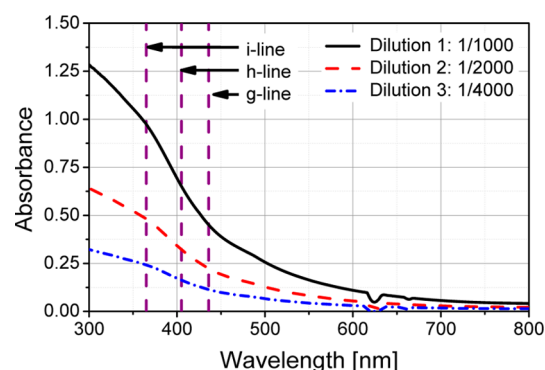
Figure 2. UV–vis spectra of 1% vol magnetite nanoparticles dissolved in GBL. Magnetite nanoparticle solutions become more transparent at higher wavelengths. Measurements are performed against a GBL background signal in a 10 mm quartz cuvette. Reprinted with permission by © IEEE 2013.

trations. As dilutions of at least 1/1000 were necessary to obtain a detectable UV–vis signal, Beer–Lambert relation may only be used to obtain an order-of-magnitude approximation for the particle absorption of a 1% vol ferrofluid (see Table 2).

Table 2. Extrapolated Absorption Coefficients per 1% Vol Magnetite in GBL ($\alpha_{Particles}$), as Well as Absorption Coefficients of the Epon-Based Photoresist SU-8 5 ($\alpha_{SU-8\ 5}$) and PI Absorption (α_{PI}, Concentration 0.43 mg/mL As Used for Composites 4−6)

|	α [cm^{-1}]					
	$\alpha_{Particles}$ extrapolated from dilution:					
λ [nm]	1	2	3	mean	$\alpha_{SU-8\ 5}$	α_{PI}[a]
365	974.3	963.0	968.2	967 ± 5	1.8	6.4
405	651.6	645.0	651.5	650 ± 3	0.9	7.8
436	451.8	447.4	455.0	451 ± 3	0.2	12.0

[a]Extrapolated from a solution containing 0.05 mg/mL H-Nu 470.

The absorption coefficients of Epon SU-8 5 (Epon to GBL ratio similar to the composites discussed in this work; see Table 1) and H-Nu 470 are also displayed in Table 2. A qualitative comparison of the absorption data identifies the particle related absorption as the main absorption mechanism. The particle related absorption coefficient decreases with increasing wavelength, promoting the expansion of the composites' photosensitive regime toward the visible spectrum.

The average irradiation intensities emitted by the mercury short arc lamp of the utilized mask aligner have been measured to be 3.1 ± 0.3 mJ s^{-1} cm^{-2} (g-line, 436 nm), 2.4 ± 0.2 mJ^{-1} cm^{-2} (h-line, 405 nm), and 2.5 ± 0.2 mJ^{-1} cm^{-2} (i-line, 365 nm), resulting in exposure doses of 128.7 ± 3.4 mW cm^{-2} (g-line), 99.9 ± 6.8 mW cm^{-2} (h-line), and 104.4 ± 0.5 mW cm^{-2} (i-line) per exposure cycle. All results include losses introduced by the experimental setup.

For i-line sensitive composites, where only a single photoinitiator sensitive to a single wavelength is used, eqs 1−4 can be solved directly. Surface and depth cure must progress at the same speed. For composites containing H-Nu 470, i-line excitation of SbF$_6$ as well as g-, h-, and i-line excitation of H-Nu 470 takes place at the same time. Assuming
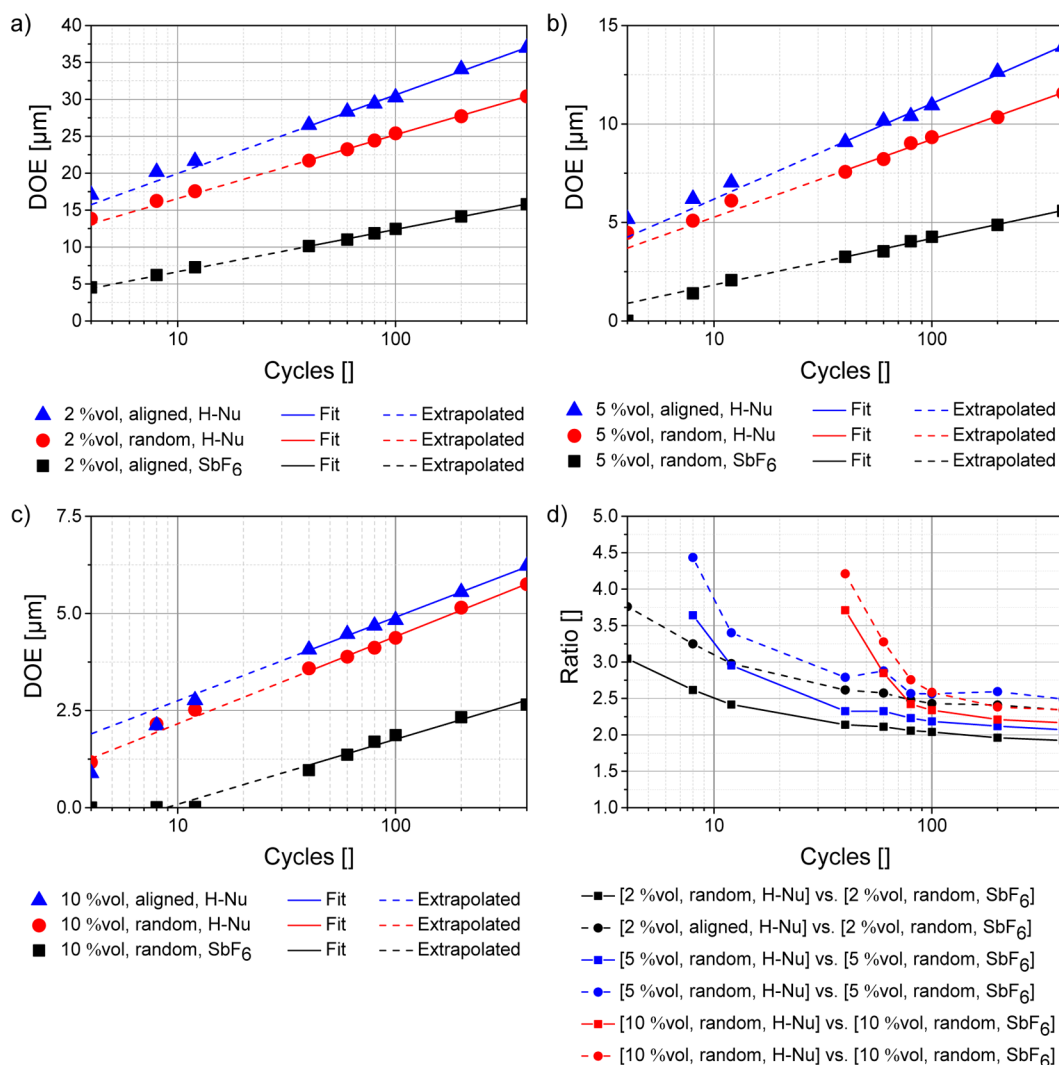
Figure 3. (a−c) Exposure kinetics of all composite films investigated in this work. (d) Exposure kinetics ratios. Average doses per cycle: g-line, 128.7 $\pm$ 3.4 mJ/cm^2; h-line, 99.9 $\pm$ 6.8 mJ/cm^2; i-line, 104.4 $\pm$ 0.5 mJ/cm^2.

Table 3. Comparison of Achieved DOE, Relative Magnetizations, Volume Saturation Magnetizations, and Apparent Particle Volume Loads^a

Load$_{V,i}$ [% vol]	active component	particle distribution	DOE rectangular [μm]	DOE circular [μm]	M_r [memu]	M_V [emu/cm^3]	Load$_V$ [% vol]
2	SbF$_6$	random	15.8 $\pm$ 0.1	17.9 $\pm$ 0.4	4.0 $\pm$ 0.1	3.6 $\pm$ 0.1	1.6 $\pm$ 0.1
	H-Nu	random	30.4 $\pm$ 0.4	33.7 $\pm$ 1.1	7.2 $\pm$ 0.5	3.3 $\pm$ 0.2	1.5 $\pm$ 0.1
	H-Nu	aligned	37.0 $\pm$ 0.1	53.5 $\pm$ 2.1	10.0 $\pm$ 0.7	3.0 $\pm$ 0.2	1.4 $\pm$ 0.1
5	SbF$_6$	random	5.6 $\pm$ 0.1	5.6 $\pm$ 0.2	3.2 $\pm$ 0.1	9.0 $\pm$ 0.2	4.1 $\pm$ 0.1
	H-Nu	random	11.6 $\pm$ 0.1	12.0 $\pm$ 0.1	6.0 $\pm$ 0.1	7.8 $\pm$ 0.1	3.6 $\pm$ 0.1
	H-Nu	aligned	13.9 $\pm$ 0.1	17.3 $\pm$ 1.2	7.7 $\pm$ 0.6	7.0 $\pm$ 0.5	3.2 $\pm$ 0.3
10	SbF$_6$	random	2.7 $\pm$ 0.1	2.6 $\pm$ 0.1	2.6 $\pm$ 0.1	15.6 $\pm$ 0.4	7.2 $\pm$ 0.2
	H-Nu	random	5.8 $\pm$ 0.1	6.1 $\pm$ 0.1	5.6 $\pm$ 0.1	14.5 $\pm$ 0.1	6.7 $\pm$ 0.1
	H-Nu	aligned	6.2 $\pm$ 0.1	6.4 $\pm$ 0.2	5.8 $\pm$ 0.2	14.3 $\pm$ 0.4	6.6 $\pm$ 0.1

^{a}All measurements were performed as triplets.

similar rate constants for both PIs and considering the FF absorption coefficients as well as the lamp irradiation intensities, g-line contribution is dominant for the depth curing of these composites, while h- and i-line contributions can be neglected. At the same time, surface curing rates are expected to increase as g-, h-, and i-line excitation takes place.

Exposure Kinetics. *Depth Cure.* The exposure kinetics of all composite films are depicted in Figure 3a−c. The related

DOE values after 400 exposure cycles are depicted in Table 3. For all composite films and exposure cycle counts above 40, a logarithmic relation between the number of cycles and the DOE can be observed as indicated by the corresponding trend line. These observations state that depth curing of these films is governed by a single dominant wavelength as discussed in the previous paragraph. The logarithmic relation between the number of cycles and the DOE also confirms that the thickness
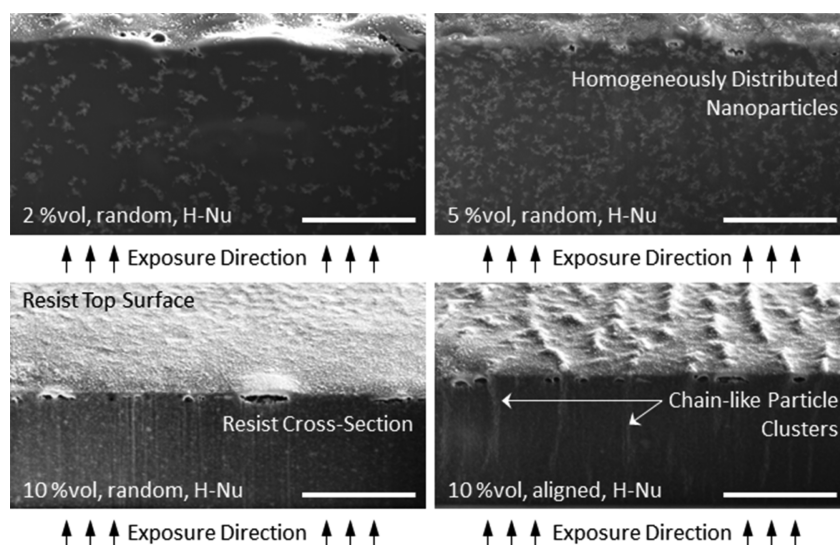
Figure 4. FIB cross section of samples differnet samples equipped with H-Nu 470 photoinitiator and random as well as aligned particle configuraions. Homogeneous particle distribution is observed for composite films that were processed in the absence of a magnetic field. Chainlike particle clusters can be observed if thermal cycling is carried out in the presence of a homogeneous magnetic field perpendicular to the surface. All scale bars are 5 μm.

of the composite films is higher than the DOE for all composite films.

Surface Cure. For cycle counts below 40, different behavior has been observed. The DOE values for all composites films containing an initial particle volume load of 10% vol (for both random and aligned particle configurations) are below the extrapolated trend line. The high concentration of particles and the resulting absorption led to an insufficient photoacid generation. For i-line sensitive composite films with random particle distributions and particle volume loads of 2% vol and 5% vol, the DOE values match the extrapolated fit, as these composites are sensitive to a single wavelength only. For visible light sensitive composites with particle loads of 2% vol and 5% vol (for both random and aligned particle configurations), the DOE values exceed the extrapolation, indicating fast surface curing due to short wavelength radiation (h- and i-line). The results are well in agreement with the general understanding of depth and surface curing mechanisms.[28]

In order to evaluate the impact of H-Nu 470 as well as impact of particle alignment on the exposure kinetics, DOE ratios are depicted in Figure 3d. DOE ratios are obtained by dividing the DOE values of two composite films of interest. The overall performance increase depends on the number of exposure cycles, the initial particle volume load, and the spatial distribution of the dispersed nanoparticles. For 400 exposure cycles, the proposed photoinitiator H-Nu 470 results in an increase in DOE of 90%, 110%, and 120% for composites with an initial particle load of 2% vol, 5% vol, and 10% vol, respectively. With decreasing exposure cycle counts, the DOE ratios increase. The related absolute DOE values are smaller, and surface curing effects become more pronounced in composite films equipped with H-Nu 470 photoinitiator, leading to an increase in DOE ratio. Similar results were obtained for composite films with aligned particles. By comparison of composite films (equipped with H-Nu 470 PI) with randomly distributed particles and films with aligned particles, the average DOE increased about 20% for films with an initial volume load of 2% vol and 5% vol and about 10% for films with an initial particle load of 10% vol.

Magnetic Properties. *Film Thickness.* VSM measurements only yield relative magnetization values. Thus, sample volumes need to be evaluated as well. The DOE values of all composites are depicted in Table 3. For composite films with homogeneously distributed particles, the DOE values are well in agreement with the ones reported for rectangular samples. However, for samples with particles aligned perpendicular to the wafer surface, DOE values are increased about 40% and 20% for composite films with an initial particle volume load of 2% vol and 5% vol, respectively. Samples used for VSM measurements were fabricated on circular 9 mm glass instead of rectangular 38 mm wafers. Because of the smaller wafer diameter, the centripetal forces on the composite are significantly smaller during spin-coating, leaving a significant edge bead behind. This edge bead reflows almost immediately after spin-coating, leading to a greatly increased film thickness. The increased film thickness implies an increased diffusion length for the solvent molecules during subsequent soft-bake. As the solidification of the composite is prolonged, the formation of particle chains is more pronounced, leading to a decrease in optical absorption and subsequently to an increase in DOE.

Absolute Sample Magnetization. The magnetic properties of all circular samples are obtained by performing VSM measurements (see Table 3). By comparison of the mean of the absolute saturation magnetization of composite films without visible light sensitive photoinitiator, the absolute saturation magnetization decreases with increasing particle load. This observation is in contradiction to the assumption derived in eq 8 and yields direct evidence that Beer−Lambert law is violated; i.e., the optical absorption must increase with increasing particle load in a nonlinear manner. This observation has a significant, counterintuitive implication on the design of future superparamagnetic sensors and actuators: If the thickness of the composite film is not restricted, the highest overall saturation magnetization is achieved using composites with reduced particle load as opposed to composites with a high particle load.

Volume Magnetization and Apparent Volume Load. Combining the DOE values and the related relative saturation

magnetization values, the volume saturation magnetization of all samples can be calculated. The results are depicted in Table 3. Comparing samples with similar initial volume load, highest volume saturation magnetization is observed for samples fabricated from composites containing SbF_6 only. Volume saturation magnetization decreases for samples fabricated from composites containing H-Nu 470. The smallest volume saturation magnetization is observed for samples with aligned particles (fabricated from composites containing H-Nu 470). By combination of the volume magnetization with extrapolated reference magnetization measurements of the iron oxide nanoparticles (217.0 emu/cm^3 or 41.8 emu/g), the measured particle volume load (see eq 7) of all composite films is calculated and depicted in Table 3. For all composite films, the measured volume load is significantly smaller than the initial volume load (see eq 9). The measured volume load of composite films with random particle distribution and SbF_6 is only about 1.1 times the measured volume load of the corresponding composite films equipped with the visible light sensitive photoinitiator H-Nu 470 and random particle distribution, indicating a systematic difference attributed to the utilization of the different photoinitiator systems.

Comparison. Considering the presence of different apparent particle volume loads in combination with the presence of nonlinear optical absorption, the ratio between exposure depths of composites with comparable initial volume load, randomly aligned particles, and different photoinitiators is not constant but yields:

$$\frac{DOE(2\% \text{ vol, HNu})}{DOE(2\% \text{ vol, SbF}_6)} < \frac{DOE(5\% \text{ vol, HNu})}{DOE(5\% \text{ vol, SbF}_6)}$$
$$< \frac{DOE(10\% \text{ vol, HNu})}{DOE(10\% \text{ vol, SbF}_6)} \tag{10}$$

The impact of particle alignment on the DOE is evaluated by calculating the DOE ratio between composite films with aligned particles and composite films with homogeneously distributed particles (both film types are equipped with the same photoinitiator H-Nu 470). The average DOE increases 20% for composite films with 2% vol and 5% vol particle load and 10% for composite films with 10% vol particle load.

Particle Distribution. The particle distribution within different composite films is illustrated in Figure 4. For visible light sensitive composite films fabricated in the absence of a magnetic field, homogeneous particle distribution can be observed. These observations indicate that H-Nu 470 photoinitiator does not affect the particle distribution within the cross-linked composite films. In the 10% vol film that underwent magnetic particle manipulation, chainlike particle clusters perpendicular to the wafer surface are observed. This verifies a successful particle alignment achieved by applying homogeneous magnetic fields during device fabrication. Similar results were obtained for all other composite films.

DISCUSSION AND CONCLUSION

UV−vis measurements of dispersed superparamagnetic nanoparticles have proven that the absorption in Epon based superparamagnetic polymer composites is solely governed by the absorption of the magnetite nanoparticles and moreover that the absorption of these particles decreases with increasing wavelength. This observation promoted the expansion of the composite's photosensitive regime toward the visible spectrum. Subsequently, we have introduced the visible light sensitive PI

H-Nu 470 to superparamagnetic polymer composites with a particle load of 2% vol, 5% vol, and 10% vol. We were able to more than double the exposure depth while maintaining the particle load (e.g., 5% vol, random, SbF_6 vs 5% vol, random, H-Nu) and to double the particle load while maintaining the resist thickness (e.g., 5% vol, random, SbF_6 vs 10% vol, random, H-Nu). The formation of ordered nanoparticle structures has proven beneficial in increasing the cross-linking depth by more than 50% (e.g., 2% vol, random, H-Nu vs 2% vol, aligned, H-Nu vs D2-4). The combination of both approaches allows for cross-linking composite films with 2.5-fold magnetization (e.g., 2% vol, random, SbF_6 vs 2% vol, aligned, H-Nu). The highest overall sample magnetization has been achieved using composites with the least filling level (2% vol, aligned, H-Nu, 10 memu) instead of composites with the highest filling level (10% vol, aligned, H-Nu, 5.8 memu). The introduction of the visible light sensitive photoinitiator H-Nu 470 and the formation of ordered nanoparticle structures have proven as effective means to increase the exposure depth limitation in superparamagnetic polymer composites. The combination of both can be exploited to fabricate superparamagnetic sensors and actuators with increased performance, narrowing the margin between composite devices and those fabricated from bulk magnetic material. These findings can further be applied to increase the lithographic performance of any other photosensitive polymer composite containing highly absorbent filler materials such as carbon nanotubes or graphene.

Superparamagnetic magnetite nanoparticles are prone to oxidation, forming maghemite (Fe_2O_3), resulting in a decreased magnetic performance. Oxidation may take place during composite processing, film storage, and potential application. In order to convincingly demonstrate the potential of superparamagnetic composite actuators for practical, long-term applications, these issues must be addressed in future research.

AUTHOR INFORMATION

Corresponding Author
*E-mail: chpeters@ethz.ch. Phone: +41 (0) 44 633 91 14.

Present Address
$^\perp$G.A.S.: Department of Environmental Health, Harvard University, 665 Huntington Avenue, Boston, MA, U.S. E-mail: sotiriou@hsph.harvard.edu.

Author Contributions
The manuscript was written by C. Peters. All authors have given approval to the final version of the manuscript. C. Peters prepared all superparamagnetic polymer composites discussed in this work and carried out the experimental work concerned with the composite's optical properties, the exposure kinetics, and the particle manipulation. O. Ergeneman carried out the magnetic characterization. H. Choi prepared the FIB cross-sectional images. O. Ergeneman, G. A. Sotiriou, B. J. Nelson, and C. Hierold supervised the project and gave critical input toward the theoretical and practical realization of the work.

Notes
The authors declare no competing financial interest.

#O.E.: e-mail, olgac.ergeneman@iris.mavt.ethz.ch.
∞H.S.: e-mail, mems@dgist.ac.kr.
×B.J.N.: e-mail, bradley.nelson@iris.mavt.ethz.ch.
○C.H.: e-mail, hierold@micro.mavt.ethz.ch.

■ REFERENCES

(1) Atkinson, G. M.; Ounaies, Z. Polymer Microsystems: Materials and Fabrication. In *The MEMS Handbook*, 2nd ed.; Gad-el-Hak, M.,Ed.; CRC Press: Boca Raton, FL, 2005; Vol. 2, Chapter 9.

(2) Meng, E.; Zhang, X.; Benard, W. Additive Processes for Polymeric Materials. In *MEMS Materials and Processes Handbook*; Ghodssi, R.; Lin, P., Eds.; Springer US: New York, 2011; Vol. 1, pp 193−271.

(3) Charles, E. C. Copolymerization. In *Seymour/Carraher's Polymer Chemistry*, 7th ed.; CRC Press: Boca Raton, FL, 2007.

(4) Jiguet, S.; Bertsch, A.; Hofmann, H.; Renaud, P. Conductive SU8 Photoresist for Microfabrication. *Adv. Funct. Mater.* 2005, 15, 1511−1516.

(5) Vescovo, L.; Sangermano, M.; Scarazzini, R.; Kortaberria, G.; Mondragon, I. In-Situ-Synthetized Silver/Epoxy Nanocomposites: Electrical Characterization by Means of Dielectric Spectroscopy. *Macromol. Chem. Phys.* 2010, 211, 1933−1939.

(6) Jiguet, S.; Bertsch, A.; Judelewicz, M.; Hofmann, H.; Renaud, P. SU-8 Nanocomposite Photoresist with Low Stress Properties for Microfabrication Applications. *Microelectron. Eng.* 2006, 83, 1966−1970.

(7) García, E. J.; Hart, A. J.; Wardle, B. L.; Slocum, A. H. Fabrication and Nanocompression Testing of Aligned Carbon-Nanotube−Polymer Nanocomposites. *Adv. Mater.* 2007, 19, 2151−2156.

(8) Lo, C.-T.; Lin, W.-T. Effect of Rod Length on the Morphology of Block Copolymer/Magnetic Nanorod Composites. *J. Phys. Chem. B* 2013, 117, 5261−5270.

(9) Metwalli, E.; Körstgens, V.; Schlage, K.; Meier, R.; Kaune, G.; Buffet, A.; Couet, S.; Roth, S. V.; Röhlsberger, R.; Müller-Buschbaum, P. Cobalt Nanoparticles Growth on a Block Copolymer Thin Film: A Time-Resolved GISAXS Study. *Langmuir* 2013, 29, 6331−6340.

(10) Metwalli, E.; Krisch, I.; Markovits, I.; Rawolle, M.; Ruderer, M. A.; Guo, S.; Wyrzgol, S.; Jentys, A.; Perlich, J.; Lercher, J. A.; Müller-Buschbaum, P. Polymer-Coated PtCo Nanoparticles Deposited on Diblock Copolymer Templates: Chemical Selectivity versus Topographical Effects. *ChemPhysChem* 2014, 15, 2236−2239.

(11) Yao, Y.; Metwalli, E.; Moulin, J.-F.; Su, B.; Opel, M.; Müller-Buschbaum, P. Self-Assembly of Diblock Copolymer−Maghemite Nanoparticle Hybrid Thin Films. *ACS Appl. Mater. Interfaces* 2014, 6, 18152−18162.

(12) Suter, M.; Ergeneman, O.; Zürcher, J.; Moitzi, C.; Pané, S.; Rudin, T.; Pratsinis, S. E.; Nelson, B. J.; Hierold, C. A Photopatternable Superparamagnetic Nanocomposite: Material Characterization and Fabrication of Microstructures. *Sens. Actuators, B* 2011, 156, 433−443.

(13) Peters, C.; Ergeneman, O.; Nelson, B. J.; Hierold, C. Superparamagnetic Swimming Microrobots with Adjusted Magnetic Anisotropy. *Micro Electro Mechanical Systems (MEMS)*, 2013 IEEE 26th International Conference, Jan 20−24, 2013; IEEE, 2013; pp 564−567.

(14) Peters, C.; Ergeneman, O.; García, P. D. W.; Müller, M.; Pané, S.; Nelson, B. J.; Hierold, C. Superparamagnetic Twist-Type Actuators with Shape-Independent Magnetic Properties and Surface Function-alization for Advanced Biomedical Applications. *Adv. Funct. Mater.* 2014, 24, 5269−5276.

(15) Suter, M.; Zhang, L.; Siringil, E.; Peters, C.; Luehmann, T.; Ergeneman, O.; Peyer, K.; Nelson, B.; Hierold, C. Superparamagnetic Microrobots: Fabrication by Two-Photon Polymerization and Biocompatibility. *Biomed. Microdevices* 2013, 1−7.

(16) Abbott, J. J.; Ergeneman, O.; Kummer, M. P.; Hirt, A. M.; Nelson, B. J. Modeling Magnetic Torque and Force for Controlled Manipulation of Soft-Magnetic Bodies. *Robotics, IEEE Trans.* 2007, 23, 1247−1252.

(17) Suter, M.; Ergeneman, O.; Zürcher, J.; Schmid, S.; Camenzind, A.; Nelson, B. J.; Hierold, C. Superparamagnetic Photocurable Nanocomposite for the Fabrication of Microcantilevers. *J. Micromech. Microeng.* 2011, 21, 025023.

(18) Gach, P. C.; Sims, C. E.; Allbritton, N. L. Transparent Magnetic Photoresists for Bioanalytical Applications. *Biomaterials* 2010, 31, 8810−8817.

(19) Ergeneman, O.; Suter, M.; Chatzipirpiridis, G.; Sivaraman, K. M.; Eberle, P.; Pané, S.; Pellicer, E.; Sort, J.; Nelson, B. J. Cobalt−Nickel Microcantilevers for Biosensing. *J. Intell. Mater. Syst. Struct.* 2013, 24, 2215−2220.

(20) Yang, S.; Megens, M.; Aizenberg, J.; Wiltzius, P.; Chaikin, P. M.; Russel, W. B. Creating Periodic Three-Dimensional Structures by Multibeam Interference of Visible Laser. *Chem. Mater.* 2002, 14, 2831−2833.

(21) Lin, Y.; Herman, P. R.; Darmawikarta, K. Design and Holographic Fabrication of Tetragonal and Cubic Photonic Crystals with Phase Mask: Toward the Mass-Production of Three-Dimensional Photonic Crystals. *Appl. Phys. Lett.* 2005, 86, 071117-3.

(22) Lv, R.-q.; Zhao, Y.; Xu, N.; Li, H. Research on the Microstructure and Transmission Characteristics of Magnetic Fluids Film Based on the Monte Carlo Method. *J. Magn. Magn. Mater.* 2013, 337−338, 23−28.

(23) Xuan, Y.; Li, Q.; Li, B. Numerical Simulation Method of Microstructure and Optical Characteristics of Magnetic Fluids. *First International Conference on Integration and Commercialization of Micro and Nanosystems, Parts A and B*, Sanya, Hainan, China; ASME: Sanya, Hainan, China, 2007; pp 1087−1094.

(24) Mack, C. Chemically Amplified Resists: Exposure and Bake Chemistry. In *Fundamental Principles of Optical Lithography*; John Wiley & Sons, Ltd.: Chichester, U.K., 2007; pp 223−256.

(25) Mack, C. Conventional Resists: Exposure and Bake Chemistry. In *Fundamental Principles of Optical Lithography*; John Wiley & Sons, Ltd: Chichester, U.K., 2007; pp 191−222.

(26) Feng, R.; Farris, R. J. Influence of processing conditions on the thermal and mechanical properties of SU8 negative photoresist coatings. *J. Micromech. Microeng.* 2003, 13, 80.

(27) Lorenz, H.; Despont, M.; Fahrni, N.; Brugger, J.; Vettiger, P.; Renaud, P. High-Aspect-Ratio, Ultrathick, Negative-Tone Near-UV Photoresist and Its Applications for MEMS. *Sens. Actuators, A* 1998, 64, 33−39.

(28) Green, W. A. Let There Be Light. *Industrial Photoinitiators: A Technical Guide*; CRC Press: Boca Raton, FL, 2010; pp 1−16.